Energy 245 (2022) 123264

Contents lists available at ScienceDirect

Energy

journal homepage: www.elsevier.com/locate/energy

Atomistic insight into oil displacement on rough surface by Janus nanoparticles

Yuanhao Chang, Senbo Xiao**, Rui Ma, Zhiliang Zhang, Jianying He*

Department of Structural Engineering, Norwegian University of Science and Technology (NTNU), 7491, Trondheim, Norway

ARTICLE INFO

Article history:
Received 24 July 2021
Received in revised form
18 January 2022
Accepted 19 January 2022
Available online 21 January 2022

Keywords:
Janus nanoparticles
Oil recovery
Molecular dynamics simulation
Rough surface
Wettability alteration

ABSTRACT

Janus nanoparticles (NPs) hold great potential in enhanced oil recovery (EOR), although the mechanism remains unclear. In the study, the displacement dynamics of trapped oil in the rough channel by Janus NPs are unraveled through atomistic modeling. The results indicate that Janus NPs with large polar faces significantly recover more oil from the nano-pocket (nano groove of the surface). The structure of adsorbed NPs on the wall of oil-trapping nano-pockets strongly causes the local wettability alteration, which ultimately determines the oil recovery. The crucial events in oil recovery by Janus NPs, termed 'adsorption invasion process', are identified, which comprise of anchoring onto the surface, pinning at the edge, and entering inside the pocket. The controlling factors are further detailed, including identification of the residual oil, displacement pressure, and the geometry of the oil-water interface inside nano-pockets. With the proposed analysis, the "huff-n-puff" mode is verified as the optimized application method for Janus NPs. For the first time, our results bring to light the dynamic wettability alteration on the rough surface by Janus NPs from atomistic insights. The findings reveal the intrinsic EOR mechanism of Janus NPs, which could guide the design and application of Janus NPs in EOR.

1. Introduction

It is expected that global energy consumption will increase by 30% or more by 2040, led mainly by fossil fuels [1]. Owing to the aggressive exploration of easily recoverable oil by the primary and secondary flooding, the current high cost and low efficiency in oil recovery have been calling for the new generation of economical and effective enhanced oil recovery (EOR) technologies, for the purpose of extracting the huge amount of remaining oil in the available reservoirs [2–4]. Such desires are greatly driven by the huge challenges encountered by the traditional oil recovery methods, including but not limited to high energy and chemicals cost, gravity override, fingering and early breakthrough, formation damage, etc. [5–7]. On addressing the challenges, nanoparticles (NPs) are believed to possess promising potentials, thanks to their ultra-small size, high surface-to-volume ratio, low costs, and environmental friendliness [8–10]. Utilizing nanofluids, namely flooding liquids with NPs, has been a focus of interest in petroleum research and applications starting from the end of the last century [11–14].

The promising EOR effect of nanofluid flooding has been confirmed in multi-scale experiments [15,16], and also in a number of field trials in Colombia, Saudi Arabia, and China [17–19]. Accordingly, multiple possible mechanisms for the nanofluid EOR, including wettability alteration, interfacial tension (IFT) reduction, structural disjoining pressure, and viscosity adjustment, have been proposed in different studies [9,20]. However, because of the lack of knowledge on atomistic interactions among NPs, fluids, and rock surfaces, the intrinsic nanoscale basis for deciphering the nanofluid EOR mechanism is still missing. Furthermore, the published conclusions were obtained based on various experimental schemes, which complicated the understanding of the NP function in EOR [19]. Hence, more fundamental research inputs are urged to accelerate the wide-ranging oilfield applications for nanofluid EOR.

It is well accepted that the chemistry and distribution of functional groups on the surface determine the behavior of NPs [21,22]. With the unique characteristic properties (polarity of two distinct hydrophobic and hydrophilic parts on the surface), Janus NPs were found to play a crucial role in EOR, with application potential proven to significantly exceed unmodified NPs [23–27]. Particularly, there are a good number of studies devoted to uncovering the excellent performance of Janus NPs at the oil-water interface

* Corresponding author.
** Corresponding author.
E-mail addresses: senbo.xiao@ntnu.no (S. Xiao), jianying.he@ntnu.no (J. He).

https://doi.org/10.1016/j.energy.2022.123264

Abbreviations

Term	Meaning
25JNP	Janus nanoparticle with nonpolar beads covering 25%
50JNP	Janus nanoparticle with nonpolar beads covering 50%
75JNP	Janus nanoparticle with nonpolar beads covering 75%
DPD	Dissipative particle dynamics
EOR	Enhance oil recovery
IFT	Interfacial tension
JNP	Janus nanoparticle
LJ	Lennard-Jones
mW	Monoatomic water
MD	Molecular dynamics
NEMD	Non-equilibrium molecular dynamics
PMF	Potential of mean force
SW	Stillinger–Weber
TraPPE-UA	The Transferable Potentials for Phase Equilibria united-atom

[27–32]. Janus NPs were proved to be more effective in the reduction of IFT if compared with other NPs with similar sizes [32]. Using dissipative particle dynamics simulations (DPD), A. Striolo et al. presented that the reduction of the IFT was determined by the surface coverage, shape, and ratio of polar/nonpolar beads of Janus NPs [29–31]. To the best of our knowledge, Wang X et al. carried out the only reported molecular study on the interactions between Janus NPs, fluids, and solid substrate [28]. Their results indicated that Janus NPs were able to hinder the oil displacement and capillary pressure was found to be the crucial factor of the process. Nevertheless, the above results were obtained in smooth channels, which could potentially be deviating or even invalid in channels with rough surfaces in real reservoirs [33–35]. Elucidating the EOR mechanisms of displacing trapped oil on rough surfaces is highly desired [36], especially with the injection of Janus NPs.

Herein, molecular dynamics (MD) simulations were employed to investigate the displacement of residual trapped oil in the rough channel by Janus NPs. Specifically, oil recovery efficiency of Janus NPs with varied fractions of nonpolar beads on the surface was presented. The detailed motion characteristics of Janus NPs on anchoring onto the solid surface, sweeping trapped oil, pinning, and entering oil trapping pockets were revealed. Crucial parameters for optimizing the EOR effect of Janus NPs were proposed. The findings of the study open out the residual oil recovery mechanism on the rough surface and are thus desired by the design and application of Janus NPs in EOR.

2. Model and simulation details

All the MD simulations were carried out using the LAMMPS package [37]. The visualization and analysis were implemented with the OVITO software [38]. As shown in Fig. 1, the atomic system representing the important feature of trapped oil on the rough surface was constructed. It had periodic boundaries and contained residual trapped oil in a nano-pocket and nanofluids. The grooved surface, namely the nano-pocket with the dimensions of $100 \times 70 \times 51$ Å^3, was created by removing the atoms in the solid substrate of silicon crystals. In order to eliminate periodic effects, the minimum height of the surface was set as 11 Å, which was

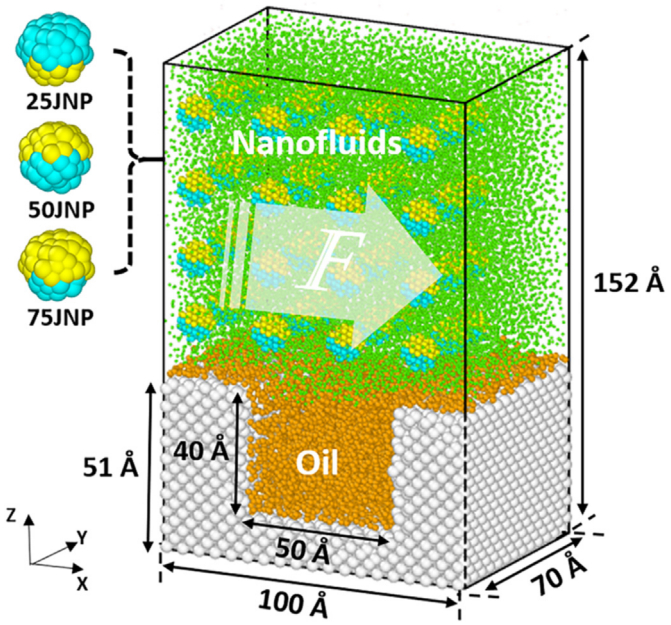

Fig. 1. The initial structure of the simulation system. The white arrow shows the flooding direction. The colors for different components: water (green), oil (orange), surface (white), the hydrophobic part (yellow), and the hydrophilic part of Janus NP (blue).

larger than the cutoff distance (10 Å). The height of residual oil film on the upper surface was around 5 Å. A number of 1004 hexane molecules were absorbed on the solid surface and in the nano-pocket to mimic the residual trapped oil after initial water flooding and had an oil density same as experiments. For the flooding phase, 48 spherical Janus NPs with a diameter of 10 Å and 21,399 water molecules were used for constructing the nanofluid with an NP concentration of 3.9%. The initial pressure was around 24.6 MPa. Three systems, with Janus NPs of the varied ratio of nonpolar beads covering 25%, 50%, and 75% of the surface areas, were built, respectively. The three corresponding Janus particle types were termed the 25JNP, the 50JNP, and the 75JNP in the following text if not otherwise specified.

The mW water model was employed for the water molecules while the Transferable Potentials for Phase Equilibria united-atom (TraPPE-UA) description of hexane is chosen for oil molecules. The mW is able to reproduce the important properties of water (like energetics, density, and structure) with better accuracy than most other water models, at an extremely low computational cost [39]. The TraPPE-UA is well suitable for the phase separation process involving alkanes by using pseudo-atoms [40]. To be specific, the mW water model used the Stillinger–Weber (SW) potential to feature the many-body non-bonded interactions, while the water-oil and oil-oil non-bonded interactions adopted the standard pairwise 12-6 Lennard-Jones (LJ) potential. In our simulation, the main purpose is to study the displacement dynamics of the residual oil by JNPs on the oil-wet surface, rather than demonstrating a designed material of JNPs or the influence of the specific surface. Therefore, materials for the surface and JNPs were not specified in the work. Based on our previous study [41], the characteristic energy ε_{ws} (water-surface) was set as 0.3 kcal/mol to form a hydrophobic surface. The characteristic energy for interactions involved by Janus NPs was selected with reference to other previous studies [28,42], with the specific values listed in supporting information Table S1.

In carrying out simulations, the systems were first energy-

minimized using the steepest descent method and followed by a 0.5-ns equilibrium stage in the NVT ensemble at 350 K. The Nosé–Hoover thermostat with a coupling coefficient of 100 fs was used to maintain the aimed temperature [43,44]. In order to mimic the nanofluid flooding process, another 60-ns non-equilibrium MD simulation (NEMD) was conducted in each system. A constant force along the x-axis (0.01 kcal/mol/Å in the reference system) was applied to each atom of water molecules. Besides, to speed up the simulation, Janus NPs were treated as the rigid body and the rough surface was positionally fixed. Five independent simulations were run for each system to improve the accuracy of results.

3. Result and discussion

3.1. Displacement of residual oil in nano pockets

The inclusion of Janus NPs into the flooding significantly affected the displacement of the trapped oil in the nano-pocket. As the snapshots of residual oil in the nano-pocket shown in Fig. 2, pure water flooding (JNP-free) led to an almost non-observable displacement effect. In contrast, Janus NPs actively interacted with the solid substrate and the trapped oil during the flooding, not only adsorbing on the rough surface but also invading into the oil pocket depending on the surface nonpolar bead ratio. 25JNPs adsorbed on the solid substrate and were able to enter the nano-pocket along the solid wall. Thanks to the large area of the polar bead on the surface, 25JNPs also brought water molecules into the nano-pocket and extracted a significant amount of oil molecules out of the pocket. The 50JNP also featured the behavior of the 25JNP in oil recovery. Furthermore, 50JNPs greatly altered the oil-water interface tension in the nano-pocket by stably dwelling at the oil-water interface [26]. 75JNPs entered the oil-trapping nano-pocket by immersion into the oil phase, thanks to the large portion of surface nonpolar beads. As such, a certain amount of oil molecules was displaced by 75JNPs due to volume exclusion in the nano-pocket.

Because of the different behaviors of Janus particle types detailed above, the final performance of oil recovery varied correspondingly. The recovery efficiency defined by the percentage of oil molecules displaced out of the nano-pocket at the end of the simulations was shown in Fig. 3(a). The 25JNP and the 50JNP possessed the most obvious displacement effect, yielding a recovery efficiency of ~34.7% and ~36.9%, respectively. In comparison, the 75JNP showed a much lower recovery efficiency of ~8%. Pure water flooding resulted in the lowest recovery efficiency (~1.7%) as expected given that the mobility of residual trapped oil was known to be highly limited after primary and secondary flooding [45,46]. The surface properties of the Janus NPs determined their final distribution in the nano-pocket after flooding. As shown in Fig. 3(b, left panel), all the Janus NPs favored accumulating on the left-side wall of the nano-pocket. Both 50 JNPs and 75JNPs appeared in the center of the nano-pocket, as they either adsorbed at the oil-water interface or immersed into the oil phase. In contrast, there were almost no 25JNPs in the center of the nano-pocket. The three kinds of Janus NPs also exhibited varied migration depth into the nano-pocket, as depicted in Fig. 3(b, right panel). The bigger the surface nonpolar area, the deeper invasion of the NPs into the nano-pocket, given the same flooding condition. Obviously, the distinct motion patterns and adsorption positions of Janus NPs underlay the displacement mechanism and subsequently the recovery efficiency, which will be discussed in detail in the following sections.

3.2. Migration characteristics of Janus NPs

3.2.1. The structure of adsorbed NPs on the wall of the nano-pocket

The migration of Janus NPs into the nano-pocket along the solid wall underpinned recovery of trapped oil, either by leading invasion of water, alteration of the oil-water interface, or simply volume exclusion as discussed above. Hence, it is of great importance to further characterize the linkage between the dynamic oil recovery, illustrated by the real-time oil molecule numbers in Fig. 4(a), and the change in the distribution and the behavior of the NPs in the

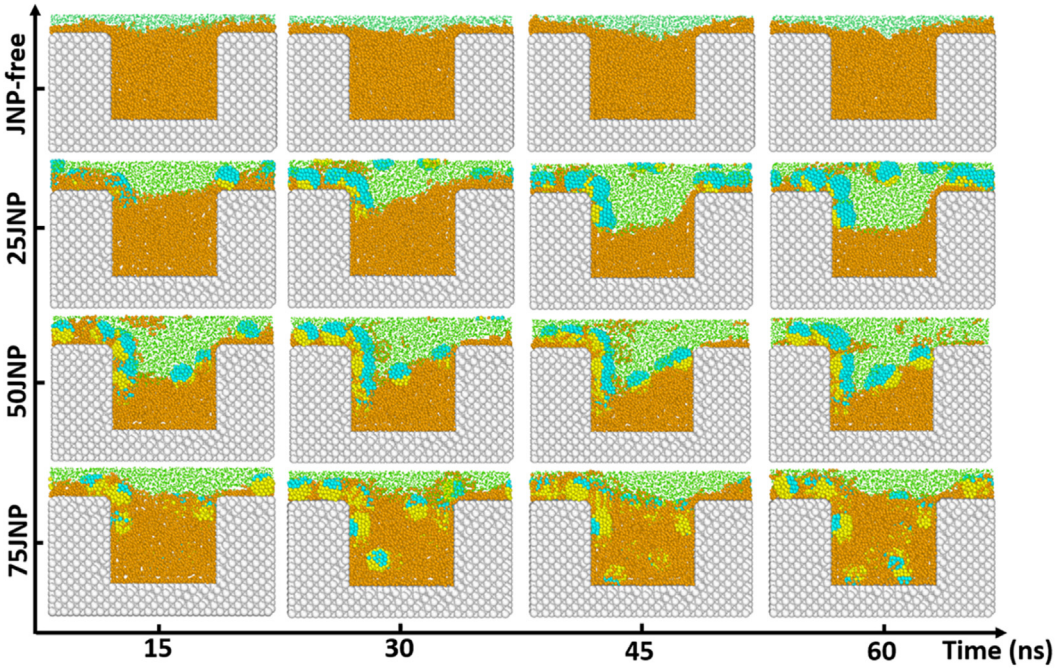

Fig. 2. System snapshots of the displacement process with different flooding. The x-axis indicates the simulation time, and the y-axis represents the types of injected Janus NPs. For better visualization, only the area near the nano-pocket was shown in the snapshots.

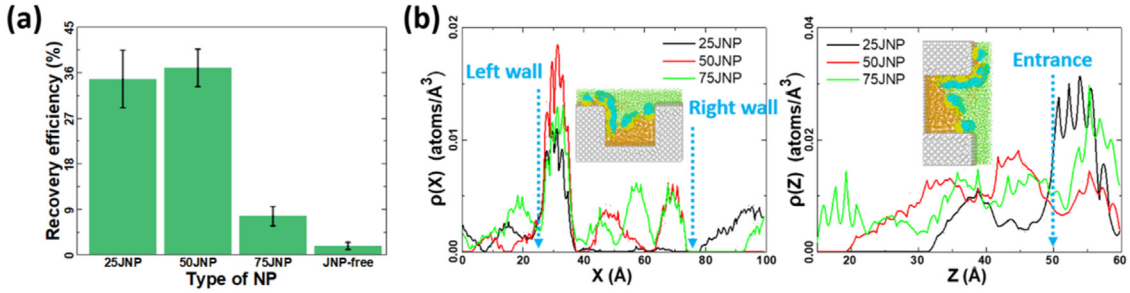

Fig. 3. Oil recovery efficiency and NPs distribution. (a) Recovery efficiency with different types of Janus NPs; (b) Distribution of NPs, quantifying by the density profiles of the atoms belong to the Janus NPs along the flooding direction (x-axis, left panel) and the depth of the nano-pocket (z-axis, right panel), respectively. The position of the walls and the entrance of the nano-pocket were marked in the figure. Representative system snapshots were shown as the inset with different perspectives for visualization.

nano-pocket in Fig. 4(c). Three quantities were adopted here for the analysis of the NPs' structure, namely the surface coverage φ of the pocket wall, the average centroid depth D, and the ratio of hydrophilicity $R_{hydrophilic}$. The detailed definitions of the three quantities were given below, with the sketch given by the snapshot in Fig. 4(b).

The surface coverage φ reflects the adsorption quantity of the NPs on the wall of the nano-pocket (Fig. 4(c, ①)), which is calculated as:

$$\varphi = \frac{N \times \pi d^2}{4A} \tag{1}$$

where N is the number of adsorbed NPs, d is the diameter of NPs and A is the surface area of the wall (dotted area in Fig. 4(c)). The higher the φ value, the more NPs adsorbed and migrated on the solid wall inside the nano-pocket. For all the Janus NPs, φ featured an obvious increasing pattern during the displacement process, with the 50JNP being the most outperforming in reaching a saturated plateau and in the number of absorbed NPs (Fig. 4(c, ①)). The depth of the adsorbed NPs directly quantifies the migration of the NPs along the solid wall into the nano pocket, which was characterized by the average centroid depth D. As shown by Fig. 4(c, ②), all the Janus NPs gradually moved down inside the nano-pocket during the displacement. 50JNPs were able to migrate the deepest distance at the end of the displacement. Interestingly, the 50JNP took the shortest time to reach the deepest position in the nano-pocket (Fig. 4 (c, ②)) and the highest φ value (Fig. 4(c, ①)), which directly resulted in the highly effective oil displacement (Fig. 4(a)). The orientation of the NPs adsorbed on the solid wall directly caused the local surface wettability alteration. The solid substrate was parameterized to be relatively hydrophobic in this work. As such, adsorbed Janus NPs with their polar faces toward the liquid phase resulted in an increase of hydrophilicity of the surface, namely making the surface more water-like. The contribution of the Janus NPs in wettability alteration was indicated by the ratio of hydrophilicity $R_{hydrophilic}$, which is defined as:

$$R_{hydrophilic} = \frac{V_{hydrophilic}}{V_{half}} \tag{2}$$

As sketched in Fig. 4(b), $V_{hydrophilic}$ accounts for the volume of the hydrophilic (polar) beads in the half of NPs, V_{half} , away from the solid wall. Taking the 50JNP for example, the $R_{hydrophilic}$ would have a value of 0 or 1 if the polar and nonpolar faces cross-section surface was parallel to the solid wall and the polar faces were facing to or

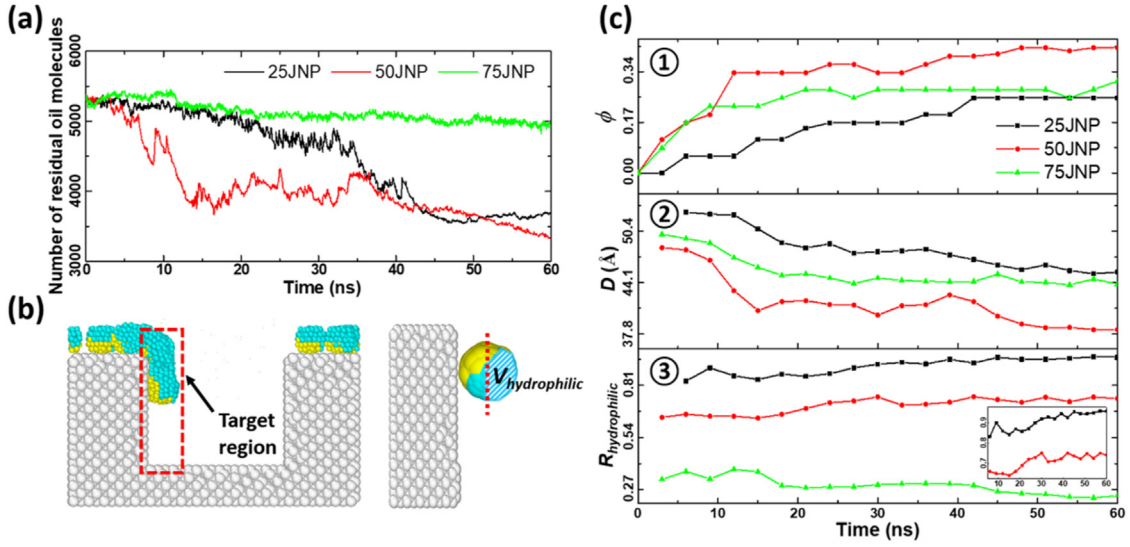

Fig. 4. Oil recovery and the underpinning behaviors of Janus NPs. (a) The number of oil molecules inside the nano pocket during the displacement. (b) Adsorption and migration of NPs on the wall of the nano-pocket and sketch of the $V_{hydrophobic}$ definition. The snapshot on the left indicated the specific NPs of interest for the analysis, and the example on the right indicated the volume of hydrophilic beads in a Janus NP used for the calculation; (c) Changes in three important quantities of the Janus NPs migrating into the nano-pocket, namely ① surface coverage, ② average centroid depth, and ③ the ratio of hydrophilicity from top to bottom.

against the solid wall, respectively. Otherwise, the $R_{hydrophilic}$ had a value between 0 and 1. Given that the 25JNP and the 75JNP were not symmetric in surface polarity like the 50JNP, the absolute value of $R_{hydrophilic}$ was not the only focus of interest for comparison but also the pattern of changes. As shown in Fig. 4(c, ③), the adsorbed 25JNPs had the highest $R_{hydrophilic}$ as expected, given their highest portion of polar beads in the NP. 50JNPs also exhibited a high value of $R_{hydrophilic}$, indicating their effectiveness in converting their adsorbing surface area into hydrophilic. Both the 25JNP and the 50JNP featured a common slowing increase pattern of $R_{hydrophilic}$ during the displacement. Despite that the 50JNP yielded an obvious lower $R_{hydrophilic}$ (0.68) than the 25JNP (0.95), their oil recovery efficiency was still superior (Fig. 4(a)), which could be attributed to more adsorbed 50JNPs on the sidewall (i.e. higher φ and lower D). The 75JNP had the lowest and a decreasing pattern of $R_{hydrophilic}$ in the three Janus NPs, owing to their relatively small polar faces. As a result, the 75JNP did not show significance in surface wettability alteration, which could be a reason for their low oil recovery (Fig. 2).

3.2.2. Motion pattern of adsorbed Janus NPs

The motion pattern of Janus NPs on the surface is the key to elaborate the mechanism of oil recovery. The Janus NPs were able to slide on the substrate and spontaneously invade into the nano-pocket, which suggested an underlying special energy landscape. To verify this phenomenon, the potential of mean force (PMF) was calculated using umbrella sampling. The PMF quantified the energy differences of one adsorbed Janus NP at different positions on the surface with the oil film without external flooding force, as the calculation system can be seen in Fig. S1. Similar to the umbrella sampling in other studies [28], the NP was anchored to positions with constant interval distances along the oil film plane by a harmonic potential for sampling in equilibration simulations. The displacement distance of the NP from its original position and the corresponding force from the harmonic potential were recorded and processed using the WHAM algorithm [47,48]. Due to the symmetry of the system, the calculation only covered the first half of the system in the x-direction. As shown in Fig. 5(a), the PMF featured fluctuations at different positions on the solid substrate and flatted out at the oil-water interface over the nano-pocket. The fluctuations of the PMF were attributed to the lattice structure effect of the substrate, namely the matching atomic structure between the Janus NPs and the surface. Good matching can lead to low energy valley of the PMF. If the atomic radius of the solid substrate increased, thus smoother surface, the amplitude of fluctuation decreased, as confirmation results showed in Fig. S2. Interestingly, there was the minimized energy at the entrance of the nano-pocket, and a subsequent high energy barrier for the Janus NPs to directly migrate along the oil-water interface over the nano-pocket, as highlighted in Fig. 5(a). Correspondingly, as indicated in Fig. 5(a), the Janus NP was stably pinned at the edge of the solid substrate. Taking the applied flooding force into consideration, such pinning effect enabled the further downward invasion of the Janus NPs into the nano-pocket and oil recovery. Without the pinned Janus NPs, the flow direction of pure water displacement at the edge of the surface didn't change much from the flooding direction. In comparison to the local streamlines of water plotted in Fig. 5(b), the adsorbed Janus NPs at the edge of the substrate altered the local wettability and resulted in the transformation of the waterflood direction. In other words, adsorbed Janus NPs on the plane solid surface and slid by the external flooding force were highly likely to stay at the rough edges of the surface and further migrate into the rough structures, which has been observed and confirmed in the experiments [49,50].

With the above analysis, the key events in the motion of Janus NPs adsorbed on the solid surface can be summarized as Fig. 6. There were four stages involved in the 'adsorption invasion process', namely oil-water interface identification and surface adsorption, edge pinning, invasion, and collision and pushing. More specifically, the Janus NPs were able to identify the oil-water interface and further adsorbed on the solid surface relying on their hydrophobic face. Driven by the flooding flow, the Janus NP slid on the surface and pinned stably at the edge of the substrate owing to the local deep energy well, termed pinning effect. Impelled by the local flooding currents, the NP initially invaded into the entrance of the nano-pocket along the solid wall. With given more Janus NPs adsorbing on the substrate and following the above route, multiple Janus NPs entered the nano-pocket and pushed the NPs in front to move down inside the nano-pocket. Owing to the unique surface wettability polarity, the Janus NPs can rotate and adjust their position in this process and alter the wettability of the solid wall. Such motion pattern resembled the appearance and growth of climbing film observed in the previous experiment [27], and provided atomistic details for a better understanding.

3.3. Controlling factors analysis

The representative motion pattern of Janus NPs on the solid surface can be specifically termed the 'adsorption invasion process' here (Fig. 6), which determined the arrangement of NPs inside the nano pocket and greatly influenced the amount of extracted oil. For a given rough surface of similar nature, three factors dominate the 'adsorption invasion process': identification of the residual oil, the driving force for migration, and geometry of oil-water interface

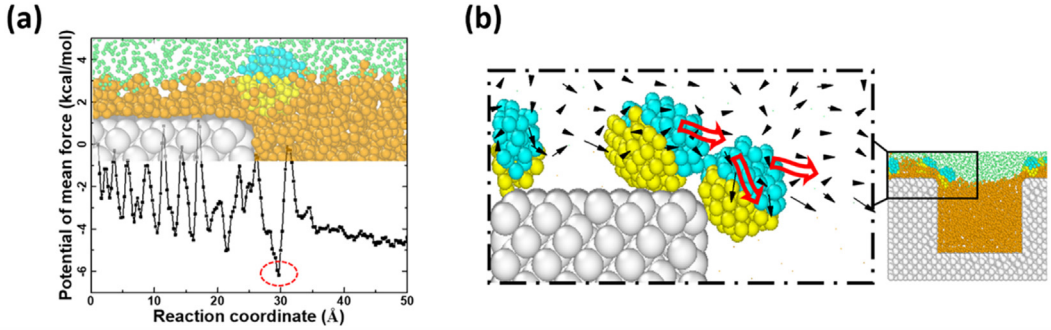

Fig. 5. Motion pattern of adsorbed Janus NPs. (a) The PMF of an NP transporting from the left side of the surface to the middle of the nano-pocket along the oil-water interface. The energy well resulting in pinning effects of Janus NPs is highlighted in the figure. (b) Local streamlines of water molecules around adsorbed Janus NPs. The red arrows indicated the motion of Janus NPs at the entrance of the nano-pocket for better visualization.

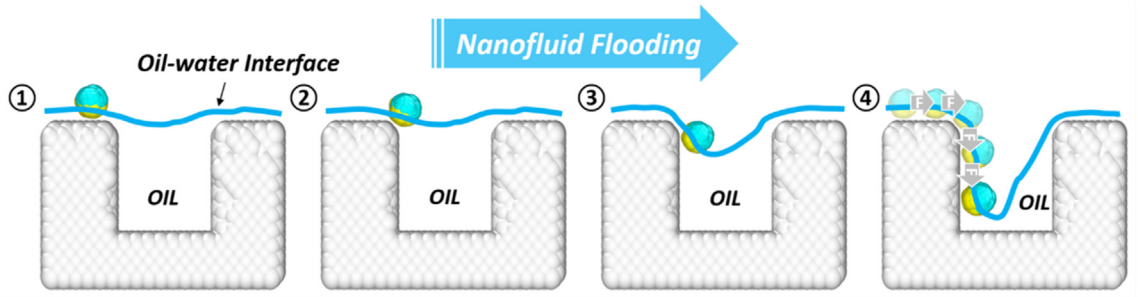

Fig. 6. Schematic diagram of the 'adsorption invasion process' of Janus NPs in the flooding. From left to right are ① oil-water interface identification and surface adsorption, ② edge pinning, ③ invasion, and ④ collision and pushing.

inside the pocket.

The 25JNP and the 50JNP behaved effectively in oil displacement, as indicated by Fig. 4, and were taken for illustrating the "adsorption invasion process" in detail. Firstly, the more Janus NPs adsorbed onto the flat substrate, the higher probability of gathering of NPs inside the nano-pocket and the higher the oil recovery. As the surface coverage of Janus NPs on the flat substrate monitored in Fig. 7(a), 50JNPs were able to adsorb and populate swiftly at the beginning of the displacement process, namely to fast identify the residual oil, which led to the fast recovery of a large number of oil molecules from the nano-pocket (Fig. 4(a)). In comparison, the 25JNP took a much longer time to populate the flat substrate area, which resulted in slower oil recovery (Fig. 4(a)). The fast adsorption of the 50JNP can be attributed to the strong interaction potential of their nonpolar faces with the oil molecules, as shown in Fig. S3. Adsorption of the 50JNP resulted in the fast decrease of the system's total energy, which was energetically favorite. In contrast, adsorption of the 25JNP led to a much less obvious contribution of system energy minimization owing to the much smaller nonpolar faces on NPs. Sufficient surface coverage of the 25JNP only happened in the later stage of displacement and subsequently the effective ongoing events of the "adsorption invasion process". Nevertheless, the high surface coverage of NPs either by the 25JNP or the 50JNP increased the collision and pushing of the fourth stage in Fig. 6, and so forth oil recovery. The encouraging result of residual oil recovery highlighted the importance of the identification of the residual oil by the Janus NPs.

The main driving force interplayed with other factors for the migration of Janus NPs, i.e., the displacement force, was also essential to oil recovery. There was an optimal threshold range of driving force, neither monotonically high nor low, for the highest oil recovery efficiency. The relationship between the applied external force and the recovery efficiency (ratio of the reduced oil molecules to the total) was recorded in Fig. 7(b), with the final system snapshots under the corresponding forces provided in Fig. S4. Under low driving forces, the Janus NPs diffused slowly and had a sufficient time to adsorb on the flat substrate. Meanwhile, the Janus NPs gained low pushing force at the pinning position at the edge of the substrate to enter the nano-pocket. On the other hand, the excessive driving force was more likely to overpower the pinning effect and forward push the NPs over the nano-pocket, in addition to decreasing the possibility of NPs adsorbing on the flat substrate. This was highly detrimental to the accumulation of NPs on the solid wall of the nano-pocket. As such, only the suitable displacement force enabled the promotion and acceleration of the 'adsorption invasion process' (Fig. 7(b)).

The alteration of the oil-water interface in the nano-pocket by the Janus NPs is worth further noting. As presented in Fig. 2, the 50JNP led to the tilted oil-water interfaces inside the nano-pocket, of which the 25JNP resulted in horizontal ones. Given the same invasion depth of Janus NPs, the horizontal oil-water interface means more oil recovery. By the analysis shown in Fig. 4(c), the most obvious wettability alteration by 25JNPs also contributed to the horizontal oil-water interface, as the large polar faces of the invaded 25JNPs encouraged more water molecules to enter the nano-pocket. It is also important to mention that the 50JNP could potentially raise NPs jamming effect in the nano-pocket. There were a considerable number of 50JNPs stably adsorbed at the oil-water interface and even at the exit edge of the nano-pocket. The accumulation of 50JNPs could further prevent the intrusion of the nearby water molecules into the nano-pocket. The less stability of the 25JNP at the oil-water interface greatly eliminated such effects.

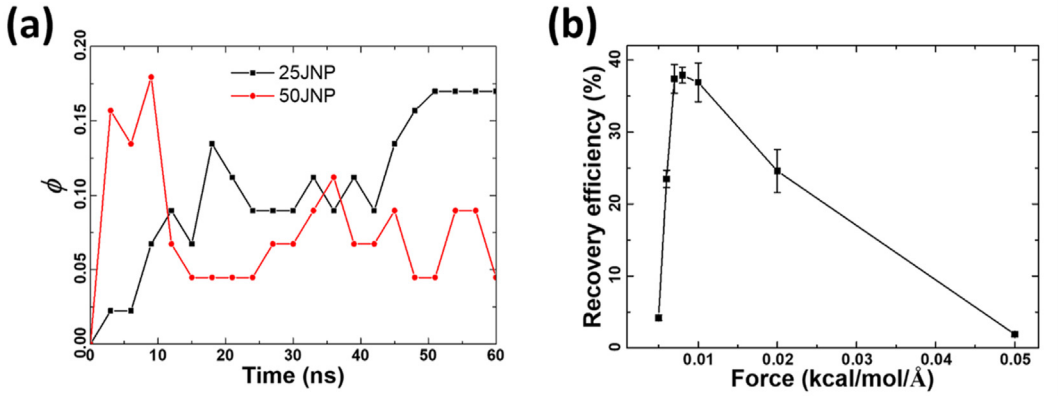

Fig. 7. Key factors determining oil recovery. (a) Dynamic surface coverage ⌀ by the 25JNP and the 50JNP on the flat substrate in the displacement. (b) The recovery efficiency by the varied applied force. The sketch solid line in the plot is for visualization.

3.4. Optimization demonstration

The results and analysis above opened rational avenues for the optimization of oil recovery. Taking the 25JNP for example, enhancing the initial adsorptions of Janus NPs on the flat substrate can improve their performance in oil recovery under the previously applied force. For demonstration, a new displacement process with the 25JNP was carried out with a 30-ns equilibration simulation for adsorption of as many 25JNPs onto the flat substrate as possible prior to applying external force. The reason for employing no external driving force in the initial stage (equilibrium stage) was that low to no displacement force contributed to the increased recognition probability of residual oil by NPs. In other words, the displacement working mode of the simulation changes from constant flooding to a cycle of "huff-n-puff". Following such an optimized flooding approach, the oil recovery effect was greatly elevated, as results shown in Fig. 8.

As shown by the change in the amount of residual oil in the nano pocket in Fig. 8(a), the optimized flooding approach promisingly increased the final oil recovery efficiency to almost 70%. For the same given flooding time under the same driving force, the optimized approach also extracted more oil than the original flooding cases. Besides the excellent oil recovery effect, the system snapshots during the displacement process shown in Fig. 8(b) further confirmed more NPs adsorbed on the flat substrate after the equilibrium simulation. Furthermore, the optimized flooding resulted in higher values of φ and $R_{hydrophilic}$ and at the same time, lower value of D by adsorbed Janus NPs (Fig. 8(c)) if compared with the original flooding (Fig. 4(c)). The results suggested that the introduction of an extra equilibration was highly beneficial for promoting the 'adsorption invasion process', which made the solid wall in the nano-pocket more hydrophilic and led to more oil recovery. The demonstration carried out using the 25JNP should apply to other Janus NPs. The "huff-n-puff" flooding approach could be a favorite operating mode for such trapped residual oil in the reservoir. As such enhancing the 'adsorption invasion process' can be a key consideration in the design of Janus NPs and the modification of flooding working mode.

4. Discussion

Atomic modeling and MD simulation provide nano-level information, especially the detailed interaction between components in the complex nanofluid system, which is formidable to obtain in large-scale oil displacement experiments. Such knowledge is essential for the design and application of JNP in nano-enabled petroleum engineering. This work adopts the coarse-grained modeling approach to achieve faster sampling by reducing the degree of freedom of the system. The selected force field has been proven to successfully reproduce the nature of the components in nanofluid systems, including physical characteristics of the fluid, the amphiphilicity of JNP, and the hydrophobicity of the surface. The modelled topography of the rough surface, here represented by the rectangular groove as in the previous studies, is able to serve the purpose of stably trapping residual oil. The periodic boundaries of the simulation systems enable an infinitely long rough surface with the trapped oil film, which is beneficial to the continuous capture and investigation of the displacement behavior of JNPs. Thus, the designed model is eligible to be a basic case for the study of the displacement of nano-scale trapped oil by JNPs, which corresponds to the nanoscale locations in the rough throats or in the internal channel of nanopores in the actual reservoir.

Unlike the previous atomistic simulations focusing on smooth channels [28], the result is more relevant to the experimental results [23–25] on deciphering the excellent EOR effect of JNP. Regarding the understanding of the EOR mechanism of JNP, previous experiments have confirmed the IFT reduction and wettability alteration caused by JNP without evaluating their contributions in the process. Giraldo et al. believe that reducing IFT is the decisive factor in this process rather than the wettability alteration [25,26]. The present work further details the dominating contribution of wettability alteration in the nanoscale oil film displacement effect. The simulations provide atomistic resolution for observing key steps of JNPs dynamics in the process of the oil-film type of residual oil displacement. Such resolution is obviously missing in the experiment where it is impossible to distinguish the specific role played by JNP for various remaining oil types

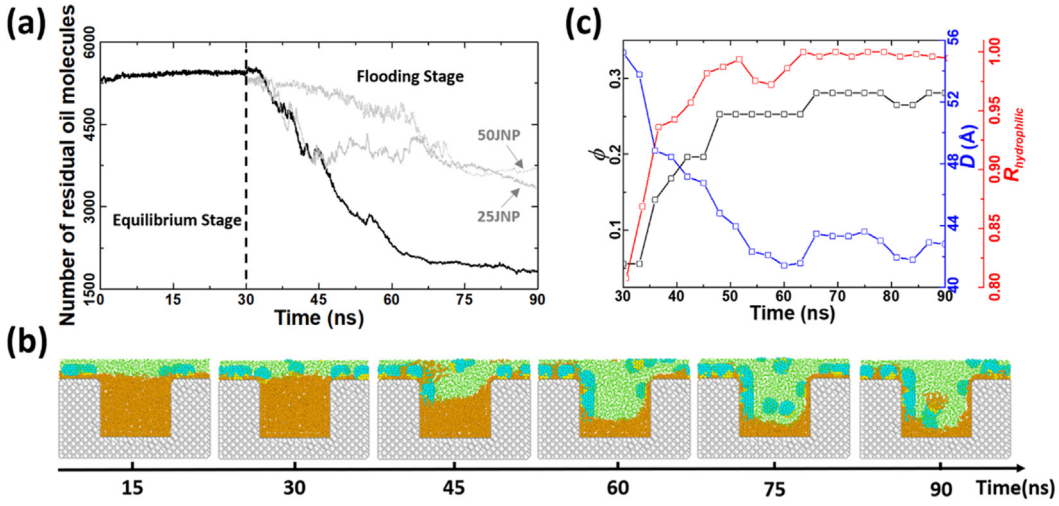

Fig. 8. The optimization approach for outperforming oil recovery. (a) The number of residual oil molecules in the nano-pocket with the injection of 25JNPs with the optimized displacement process. Performance by the 25JNP and the 50JNP in the original displacement process is shown (grey curves) for comparison. (b) System snapshots of oil exaction after optimized displacement process; (c) Dynamic surface coverage φ, centroid depth D, and the ratio of hydrophilicity $R_{hydrophilic}$ following the optimized flooding.

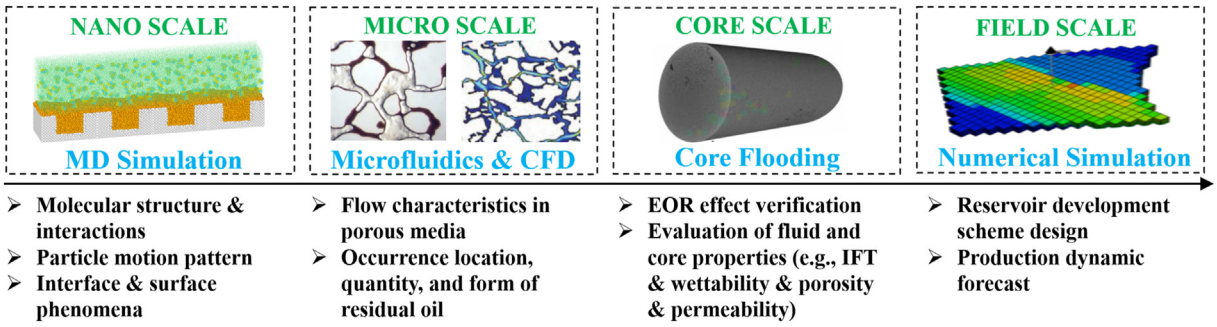

Fig. 9. The framework of the multiscale EOR research techniques. The CFD is short for Computational Fluid Dynamics.

(clustered, columnar, droplet, etc. [51]). As such, simulations of this kind provide the possibility for the refined interpretation of the EOR mechanism of JNP. Furthermore, this work reveals the dynamics of wettability alteration (ie, the 'adsorption invasion process'), which is highly valuable to nanoparticle design in EOR. Interestingly, the 'adsorption invasion process' observed in this work features the previous proposed 'climbing film' of Janus nanosheets [27]. However, the intrinsic mechanisms of the two are different. As the so-called Marangoni stress is the key to 'climbing film', the pinning effect driven by local energy minimum governs the 'adsorption invasion process' in the migration of JNP on the solid surface and into the nano-pores.

It should be noted that this work focuses on the displacement of oil film by JNPs on a rough surface with simplified parameter sets. Key factors such as oil type properties, water salinity, rock properties, the concentration of JNPs, pore geometries and size, and system temperature and pressure, await intensive investigation and discussion. Nevertheless, it is foreseeable that some of these factors have their synergy to the 'adsorption invasion process' of JNP on the EOR. Further extensive atomistic modeling and simulations are needed for answering such questions. Lastly, upscaling the results and eventually bridging them to the reservoir scale is the ultimate goal in future work. It's undeniable that the obtained motion pattern and the optimal fraction of hydrophilic parts for JNP can qualitatively guide the design and fabrication of JNP in EOR. What's more, the results can provide a design basis of the bottom layer parameters for the final effect prediction at the reservoir scale. As illustrated in the framework of the multiscale EOR research method (Fig. 9), the work contributes to the fine-tuning of the parameters for microscale experiments or fluid simulations such as roughness and JNP properties. Based on this, the microscopic study can verify the displacement effect of JNP and further extend the displacement characteristics to the core scale. Finally, the prediction of the displacement effect of JNP under actual reservoir conditions is carried out in the reservoir numerical simulation with the help of the evaluation of the performance of JNP in core flooding. Besides, combined with the increasingly mature machine learning technology, a large number of MD simulation results can also be adopted to construct a screening chart of JNP properties and displacement effects, which can be directly utilized in the design of EOR applications.

5. Conclusions

Oil recovery from the rough surface by displacement of Janus NPs was investigated using atomistic modeling and MD simulations. The study found that Janus NPs with larger polar faces (25JNPs and 50JNPs) achieved a more notable oil recovery effect than those with smaller polar faces (75JNPs) or pure water (JNP-free). The structure of adsorbed NPs on the wall of the nano-pockets strongly affected oil recovery efficiency. Altering the solid wall to be more hydrophilic by adsorbed Janus NPs can lead to deeper migration of the NPs into the nano-pocket and more oil recovery. Furthermore, an 'adsorption invasion process' was identified in this work, highlighting the key mechanism of the oil recovery effect of Janus NPs. Specifically, Janus NPs adsorbed on the solid surface by first identifying the oil-water interface. Constrained by the pinning effect, the adsorbed Janus NPs slid and stayed on the edge before entering oil trapping nano-pockets. Under the impelling local water flow, the pinned Janus NPs were forced into the nano-pocket along the solid wall. With the continuous collisions and pushing, more Janus NPs could further migrate deep into the nano-pockets. Moreover, controlling factors, including identification of the residual oil, displacement pressure, and the geometry of the oil-water interface inside nano-pockets, were proposed for the 'adsorption invasion process'. Utilizing the new results and analysis, an optimization flooding approach, namely the "huff-n-puff" working mode, was proposed, which yielded outstanding oil recovery performance. The findings of this work directly correlated critical factors with oil recovery on the rough surface by Janus NPs for the first time and shed light on the intrinsic EOR mechanism of Janus NPs. The results provided guidance not only for designing the suitable Janus NPs, but also for modifying the targeted displacement strategy in the practical applications of EOR.

Credit author contribution statement

Yuanhao Chang: Conceptualization, Writing-original draft. **Senbo Xiao**: Methodology, Software. **Rui Ma**: Software. **Zhiliang Zhang**: Writing-review & editing, Supervision. **Jianying He**: Validation, Writing-review & editing.

Declaration of competing interest

The authors declare that they have no known competing financial interests or personal relationships that could have appeared to influence the work reported in this paper.

Acknowledgments

This work was financially supported by the Research Council of Norway (Grant No. 234626) and the Chinese Scholarship Council. The supercomputer CPU hours were provided by the Norwegian Metacenter for Computational science (Project ID: NN9110K and NN9391K).

Appendix A. Supplementary data

Supplementary data to this article can be found online at https://doi.org/10.1016/j.energy.2022.123264.

References

[1] Newell R, Raimi D, Aldana G. Global Energy Outlook 2019: the next generation of energy. Resourc Future 2019:8–19.
[2] Bai B. Overview: eOR/IOR (january 2008). 42-42 J Petrol Technol 2008;60(1).
[3] Richards PW, Frankham R, Walsh R. The tropical rain forest: an ecological study. Cambridge university press; 1996.
[4] Lyons WC, Plisga GJ. Standard handbook of petroleum and natural gas engineering. Elsevier; 2011.
[5] Sun X, et al. Enhanced heavy oil recovery in thin reservoirs using foamy oil-assisted methane huff-n-puff method. Fuel 2015;159:962–73.
[6] Ahmadi Y, et al. Comprehensive Water–Alternating-Gas (WAG) injection study to evaluate the most effective method based on heavy oil recovery and asphaltene precipitation tests. J Petrol Sci Eng 2015;133:123–9.
[7] Olajire AA. Review of ASP EOR (alkaline surfactant polymer enhanced oil recovery) technology in the petroleum industry: prospects and challenges. Energy 2014;77:963–82.
[8] Haruna MA, et al. Nanoparticle modified polyacrylamide for enhanced oil recovery at harsh conditions. Fuel 2020;268:117186.
[9] Almahfood M, Bai B. The synergistic effects of nanoparticle-surfactant nanofluids in EOR applications. J Petrol Sci Eng 2018;171:196–210.
[10] Sun X, et al. Application of nanoparticles in enhanced oil recovery: a critical review of recent progress. Energies 2017;10(3):345.
[11] Chaturvedi KR, et al. Experimental investigations to evaluate surfactant role on absorption capacity of nanofluid for CO2 utilization in sustainable crude mobilization. Energy 2021;225:120321.
[12] Yang X, et al. Nanoparticle plugging prediction of shale pores: a numerical and experimental study. Energy 2020;208:118337.
[13] Khalil M, et al. Advanced nanomaterials in oil and gas industry: design, application and challenges. Appl Energy 2017;191:287–310.
[14] Murshed SS, De Castro CN. Nanofluids: synthesis, properties, and applications. Incorporated: Nova Science Publishers; 2014.
[15] Li K, Wang D, Jiang S. Review on enhanced oil recovery by nanofluids. Oil Gas Sci Technol Rev IFP Energies nouvelles 2018;73:37.
[16] Kazemzadeh Y, et al. Review on application of nanoparticles for EOR purposes: a critical review of the opportunities and challenges. Chin J Chem Eng 2019;27(2):237–46.
[17] Wilson A. Field trials of reservoir nanoparticles reveal stability, high rates of recovery. J Petrol Technol 2012;64(11):92–9.
[18] Kanj MY, Rashid M, Giannelis E. Industry first field trial of reservoir nanoagents. In: SPE Middle East oil and gas show and conference. Society of Petroleum Engineers; 2011.
[19] Yakasai F, et al. Current developments and future outlook in nanofluid flooding: a comprehensive review of various parameters influencing oil recovery mechanisms. J Ind Eng Chem 2021;93:138–62.
[20] Idogun AK, et al. A review study of oil displacement mechanisms and challenges of nanoparticle enhanced oil recovery. In: SPE Nigeria annual international conference and exhibition. OnePetro; 2016.
[21] Ruhland TM, et al. Janus cylinders at liquid–liquid interfaces. Langmuir 2011;27(16):9807–14.
[22] Laredj-Bourezg F, et al. Emulsions stabilized with organic solid particles. Colloids Surf A Physicochem Eng Asp 2012;413:252–9.
[23] Wu H, et al. Silica-based amphiphilic Janus nanofluid with improved interfacial properties for enhanced oil recovery. Colloids Surf A Physicochem Eng Asp 2020;586:124162.
[24] Liu P, et al. Functional janus-SiO2 nanoparticles prepared by a novel “cut the gordian knot” method and their potential application for enhanced oil recovery. ACS Appl Mater Interfaces 2020;12(21):24201–8.
[25] Giraldo LJ, et al. Enhanced waterflooding with NiO/SiO2 0-D Janus nanoparticles at low concentration. J Petrol Sci Eng 2019;174:40–8.
[26] Giraldo LJ. Janus nanoparticles for enhanced oil recovery EOR: reduction of interfacial tension. In: SPE annual technical conference and exhibition. Society of Petroleum Engineers; 2018.
[27] Luo D, et al. Nanofluid of graphene-based amphiphilic Janus nanosheets for tertiary or enhanced oil recovery: high performance at low concentration. Proc Natl Acad Sci Unit States Am 2016;113(28):7711–6.
[28] Wang X, et al. Transportation of Janus nanoparticles in confined nanochannels: a molecular dynamics simulation. Environ Sci: Nano 2019;6(9):2810–9.
[29] Luu XC, Striolo A. Ellipsoidal Janus nanoparticles assembled at spherical oil/water interfaces. J Phys Chem B 2014;118(47):13737–43.
[30] Luu XC, Yu J, Striolo A. Nanoparticles adsorbed at the water/oil interface: coverage and composition effects on structure and diffusion. Langmuir 2013;29(24):7221–8.
[31] Luu XC, Yu J, Striolo A. Ellipsoidal Janus nanoparticles adsorbed at the water-oil interface: some evidence of emergent behavior. J Phys Chem B 2013;117(44):13922–9.
[32] Glaser N, et al. Janus particles at liquid– liquid interfaces. Langmuir 2006;22(12):5227–9.
[33] Chang Y, et al. Displacement dynamics of trapped oil in rough channels driven by nanofluids. Fuel. 2021. p. 122760.
[34] Toghraie D, et al. Molecular dynamics simulation of Couette and Poiseuille Water-Copper nanofluid flows in rough and smooth nanochannels with different roughness configurations. Chem Phys 2019;527:110505.
[35] Alipour P, et al. Molecular dynamics simulation of fluid flow passing through a nanochannel: effects of geometric shape of roughnesses. J Mol Liq 2019;275:192–203.
[36] Fang T, et al. Oil extraction mechanism in CO2 flooding from rough surface: molecular dynamics simulation. Appl Surf Sci 2019;494:80–6.
[37] Plimpton S. Fast parallel algorithms for short-range molecular dynamics. J Comput Phys 1995;117(1):1–19.
[38] Stukowski A. Visualization and analysis of atomistic simulation data with OVITO–the Open Visualization Tool. 015012 Model Simulat Mater Sci Eng 2009;18(1).
[39] Molinero V, Moore EB. Water modeled as an intermediate element between carbon and silicon. J Phys Chem B 2009;113(13):4008–16.
[40] Martin MG, Siepmann JI. Transferable potentials for phase equilibria. 1. United-atom description of n-alkanes. J Phys Chem B 1998;102(14):2569–77.
[41] Chang Y, et al. Nanomechanical characteristics of trapped oil droplets with nanoparticles: a molecular dynamics simulation. J Petrol Sci Eng 2021:108649.
[42] Wang X, et al. Insight into the pressure-induced displacement mechanism for selecting efficient nanofluids in various capillaries. Environ Sci: Nano 2020;7(9):2785–94.
[43] Nosé S. A unified formulation of the constant temperature molecular dynamics methods. J Chem Phys 1984;81(1):511–9.
[44] Hoover WG. Canonical dynamics: equilibrium phase-space distributions. Phys Rev 1985;31(3):1695.
[45] Craig FF. The reservoir engineering aspects of waterflooding, vol. 3. New York: HL Doherty Memorial Fund of AIME; 1971.
[46] Willhite GP. Waterflooding. 1986.
[47] Choudhary N, et al. Effect of polyvinylpyrrolidone at methane hydrate-liquid water interface. Application in flow assurance and natural gas hydrate exploitation. Fuel 2016;186:613–22.
[48] Beckmann A, et al. A fast recoiling silk-like elastomer facilitates nanosecond nematocyst discharge. BMC Biol 2015;13(1):1–16.
[49] Zhang P, et al. Grooved organogel surfaces towards anisotropic sliding of water droplets. Adv Mater 2014;26(19):3131–5.
[50] Chang B, et al. Sliding droplets on hydrophilic/superhydrophobic patterned surfaces for liquid deposition. Appl Phys Lett 2016;108(15).
[51] Mi L, et al. Microscopic oil and water percolation characteristic investigation of water flood reservoir in ultrahigh water cut period. In: SPE Trinidad and Tobago section energy resources conference. OnePetro; 2016.